Poromechanics of saturated isotropic nanoporous materials

Romain Vermorel, Gilles Pijaudier-Cabot, Christelle Miqueu, Bruno Mendiboure

Chapter 1

Poromechanics of saturated isotropic nanoporous materials

Romain Vermorel, Gilles Pijaudier-Cabot, Christelle Miqueu and Bruno Mendiboure,
Laboratoire des Fluides Complexes et leurs Réservoirs (UMR 5150),
Université de Pau et des Pays de l'Adour, FRANCE.

1.1 Abstract

Poromechanics offers a consistent theoretical framework for describing the mechanical response of porous solids. When dealing with fully saturated nanoporous materials, which exhibit pores of the nanometer size, additional effects due to adsorption and confinement of the fluid molecules in the smallest pores must be accounted for. From the mechanical point of view, these phenomena result into volumetric deformations of the porous solid, the so-called "swelling" phenomenon, and into a change of the apparent permeability. The present work investigates how poromechanics may be refined in order to capture adsorption and molecular packing induced effects in nanoporous solids. The revisited formulation introduces an effective pore pressure, defined as a thermodynamic variable at the representative volume element scale (mesoscale), which is related to the mechanical work of the fluid at the pore scale (nanoscale). Accounting for the thermodynamic equilibrium of the system, this effective pore pressure is obtained as a function of the bulk fluid pressure, the temperature and the total and excess adsorbed masses of fluid. We derive the analytical swelling strains due to sorption and molecular packing. A good agreement in the comparison with experimental data dealing with the swelling of coal due to methane and carbon dioxyde sorption is observed, as a preliminary stage towards modelling partially saturated solids and applications to cement paste.

1.2 Introduction

Poromechanics offers a consistent theoretical framework for describing the mechanical response of porous solids saturated, or partially saturated with a fluid phase. The theory is based upon the superposition of the solid and liquid phases. In the case of fully saturated porous solids, it is assumed that the fluid-solid interaction is restricted to the influence of the pressure on the inner surface of

the porous material. In partially saturated porous solid, additional forces, i.e. capillary forces are introduced. Many authors have used this modern theoretical framework, which is thoroughly described e.g. in the textbooks by [5, 6].

We are going to specifically focus on "nanoporous" materials, e.g. solids with pores down to the nanometer size ($\leq 2\,\mathrm{nm}$). Hardened cement paste or tight rocks are among those materials, which can be used in construction, or may be encountered in the production of gas from very tight reservoirs or coal seams. Aside from the classical fluid-solid interaction observed in macroporous materials, there are additional effects that should be considered in such materials: (i) adsorption is important because the inner surface of the pores is very large and surface forces cannot be neglected anymore; (ii) in very small pores, the molecules of fluid are confined. Interaction between molecules of fluid is modified, it cannot develop in the same way as if the fluid would be placed in a large container. This effect, denoted as molecular packing, includes fluid-fluid and fluid-solid interactions.

From the macroscopic mechanical point of view, these phenomena result into volumetric deformations of the porous solid. Swelling is commonly observed during sorption-desorption of several gases such as carbon dioxide or methane in charcoal, see e.g. the paper by Levine [14] although seminal experimental works of Meehan [15] or Bangham and Fakhroury [1] date back to the 1920s. In the more complex context of unsaturated cement pastes, the variation of disjoining pressure due to the variation of relative humidity is one of the most probable mechanism for dessication induced shrinkage [3]. Disjoining pressures follow a similar scheme as adsorption effects, except that a gas/fluid interface is involved in addition to the solid/fluid interface. Hence, shrinkage upon dessication can be regarded as a volumetric deformation upon desorption.

In this chapter, we are going to investigate how the poromechanical theory may be refined to take account for adsoprtion and molecular packing in nanopores. In order to provide the reader with an illustration of these effects, we start with molecular simulations of a slit pore containing a simple fluid. We examine the variation of pore pressure with the bulk fluid pressure to which it is connected and with the pore width. Then, in view of the complexity of the local - atomistic - effects at this scale, we turn towards averaged, macroscopic considerations. The formulation which is thoroughly described in [23] introduces an effective pore pressure as a thermodynamical variable defined at the representative elementary volume scale. Accounting for the thermodynamic equilibrium of the system composed of the nanoporous skeleton, the interstitial and external bulk reference fluid, the relation between the effective pore pressure and quantities measurable in experiments such as the temperature, the bulk fluid pressure and the total and excess adsorbed mass of fluid is obtained. The swelling of a porous material, saturated with a simple fluid, is obtained as a function of adsorption and mechanical parameters. Finally, the case of fluid transport in such a nanoporous material is considered. A Darcy type relation is derived, in which an effective intrinsic permeability appears. This permeability is a function of the bulk fluid pressure and decreases as the bulk pressure increases.

In the illustrations, we will focus on activated carbon and coal saturated with a simple gas, which are materials rather remote to cement paste. These examples should be understood as a first step toward a formulation applicable to cement paste which is partially saturated. Physisorption is considered only and electrical effects are neglected, which is a great simplification. Also, the porous material is fully saturated, and preferential sorption is thus not considered (which is another complexity of the problem). Yet, the foregoing discussion provides some insight on the pertinence of the approach and sets the scene for more complex applications, those involved in the understanding of the time-dependent response of cement-based materials.

1.3 Results from molecular simulations

We consider a slit pore of width H as shown in Figure 1(a). Monte Carlo simulations are performed in the Grand Canonical ensemble. The fluid-fluid interactions are described with a 12-6 Lennard-Jones potential and the solid-fluid interaction by the integrated 10-4-3 potential. Numerous studies, based on molecular simulations ([16], [19], [13]) and DFT methods [24], focus on modeling the spatial variations of the fluid properties, namely the fluid density, viscosity and pore pressure, at the scale of a single nanopore. We are going to focus on the normal pressure inside the pore only. The pore pressure P is the component perpendicular to the surface of the pore. In confined fluids, the pressure is not a scalar and the tangent and normal pressures to the surface of the pore are different. The normal pressure P is computed with the Viriel estimate as described by Varnik et al. [22].

In the present calculations, the solid phase is graphite and the fluid phase is methane at 353 K. For a bulk pressure equal to 2 MPa, the evolution of the pore pressure with the pore width is plotted in Figure 1(a). Oscillations corresponding to the structuration of the fluid into layers are observed. This structuration effect result from the confinement of the fluid molecules between the two infinitely rigid pore walls. Note the range of variation of the pore pressure, with very high values for small pore sizes. Figure 1(b) shows the pore pressure versus the bulk pressure for several pore sizes. This is clearly a nonlinear relation which is very much dependent on the pore size H.

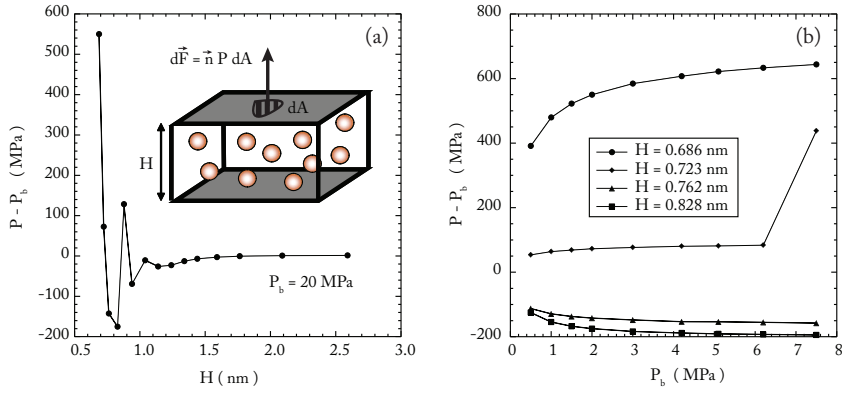

Figure 1.1: (a) Component of the pore pressure perpendicular to the pore wall versus the pore size, for a bulk pressure equal to 2 MPa (methane into graphitic slit pores at 353K). Inserted figure: Model of graphite parallel slit pore used in GCMC simulations. (b) Component of the pore pressure perpendicular to the pore wall versus bulk pressure, for different pore sizes (methane into graphitic slit pores at 353K). Dots stand for the molecular simulations results; solid lines are guides for the eyes.

In summary, the GCMC molecular simulations indicate that adsorption and confinement of the fluid molecules in the nanopores result in pressure differentials between the interstitial fluid and the external bulk solution. From the mechanical point of view, these adsorption induced pressure differentials are likely to provoke volumetric deformations of the nanoporous material. The difficulty is that the pore pressure strongly depends on the geometry of the pores and on the

pore size distribution. The smallest pores contribute the most to high pressures, only is the fluid is not ordered in the pore. Therefore, it is rather difficult to provide an overall picture of the mechanical effect of fluid confinement, upscaling results from molecular simulations directly. In the following, we are going to show how the poromechanical theory may be refined in order to take into account these singular effects in a global way, based on some energy equivalence.

1.4 Poromechanical model

In this section, we present the poromechanical model for saturated isotropic nano-porous solids. After introducing the general nomenclature and definitions, we define the effective pore pressure. Then, we derive the expressions for the dissipations following the theory of the thermodynamics of porous continua proposed by O. Coussy [5]. Referring to the principle of thermodynamical equilibrium, we derive an equation which relates the state variables of the interstitial fluid to those of the bulk external fluid.

1.4.1 Nomenclature and definitions

The porous medium is an open thermodynamic system, which consists in the superposition of a porous solid phase, the skeleton, and an interstitial fluid phase which can exchange fluid mass with the external reference bulk solution. Hence, the use of a subscript s or f refers to a variable related to the skeleton or to the interstitial fluid respectively. Moreover, the subscript b is used when referring to the bulk solution. For instance, a quantity χ, related to the phase π will write χ_π, with $\pi = f, s, b$ for the interstitial fluid, the skeleton and the bulk fluid respectively.

Poromechanics describes the behavior of a porous medium at the mesoscale of the representative elementary volume (REV) at which the different variables are defined. Though, when dealing with nanoporous solids, in which the thermodynamical state of the intersititial fluid depends locally on the pore size and geometry, quantities defined at the nanoscale of the pores are involved as well. Quantities related to the pore nanoscale are superscripted with the letter n. We emphasize that the pore scale variables appearing in this work stand for the mean quantities calculated over the volume of one pore of a specific size and geometry. For example, the pore scale fluid density ρ_f^n, which depends on the pore size and geometry, stands for the mean fluid density calculated over the volume of the pore.

The porosity is defined as the ratio of the volume of the connected pores to the total volume of the porous solid. In other words, the occluded pores are not accounted for in the definition of the porosity. In the context of nanoporous materials, the proportion of occluded porosity might depend on the nature of the saturating fluid, as only pores larger than the fluid molecules size are accessible. We note ϕ and φ the lagrangian and eulerian porosity respectively, and we write:

$$\phi = \frac{1}{\Omega_0} \int_{\Omega_0} d\Omega_0 \, \phi^p \tag{1.1}$$

$$\varphi = \frac{1}{\Omega^e} \int_{\Omega^e} d\Omega^e \, \varphi^p \tag{1.2}$$

where Ω_0 and Ω^e stand for the lagrangian and eulerian REV. ϕ^p and φ^p are, respectively, the partial lagrangian and eulerian porosity, *i.e* the porosity related to all the pores of a specific size and geometry in the REV. Relations (1) and (2) exemplify how mesoscale extensive quantities are obtained from summation of their nanoscale counterparts over the REV.

1.4.2 Effective pore pressure

Classical poromechanics account for the stress related to the skeleton and the one related to the fluid separately. In a saturated porous solid, in which no confinement effects occur, the stress partition in the eulerian frame is expressed as

$$\begin{aligned}\underline{\Sigma}^e &= (1-\varphi)\underline{\Sigma}_s^e + \varphi\underline{\Sigma}_f^e \\ &= (1-\varphi)\underline{\Sigma}_s^e - \varphi P_b \underline{\mathbb{1}}\end{aligned} \tag{1.3}$$

where $\underline{\Sigma}^e$ is the global stress tensor related to the porous continuum in the eulerian frame, $\underline{\Sigma}_s^e$ and $\underline{\Sigma}_f^e$ the skeleton and fluid stress tensors in the eulerian frame respectively, and P_b the bulk fluid pressure. Thus, the intrinsic averaged stress within the fluid is addressed through the spherical tensor $-P_b\underline{\mathbb{1}}$. This comes down to consider that the fluid applies an isotropic pressure on the pores walls, which is equal to the bulk pressure.

At the scale of the nanopores, molecular simulations clearly show that the fluid stress tensor is anisotropic and depends locally on the size and the geometrical shape of the pores. With the exception of some synthetic materials [11], nano-porous solids such as coal or cement paste usually exhibit a continuous pore size distribution, with distributed pore geometries and spatial orientations. The calculation of effective poromechanical properties based on micro-macro upscaling methods is an open problem. Existing methods are often restricted to the description of model nanoporous materials (e.g. in ref. [18]). Nevertheless, numerous experimental studies demonstrate that the sorption induced strains in nanoporous solids are isotropic as long as the material structure is isotropic [14, 7, 17]. Thus, in the case of isotropic saturated nanoporous materials, at the scale of the REV we can consider that the interstitial fluid acts as an effective fluid exerting an isotropic pore pressure P_f on the pores walls. Let us point out that the effective pore pressure may be different from the bulk fluid pressure P_b. As a result, in the nanoporous material, the stress partition writes

$$\begin{aligned}\underline{\Sigma}^e &= (1-\varphi)\underline{\Sigma}_s^e + \varphi\underline{\Sigma}_f^e \\ &= (1-\varphi)\underline{\Sigma}_s^e - \varphi P_f \underline{\mathbb{1}}.\end{aligned} \tag{1.4}$$

In the limit of small strains, the stress partition in the lagrangian frame reads [6]

$$\underline{\Sigma} = (1-\phi)\underline{\Sigma}_s - \phi P_f \underline{\mathbb{1}}. \tag{1.5}$$

Following a reasoning based on the conservation of the internal energy of the interstitial fluid, the effective pore pressure can be expressed in terms of the nanoscale variables of the fluid. Because it is an extensive quantity, the lagrangian Gibbs energy G_f of the interstitial fluid (defined per unit REV volume) may be obtained by summation over the porous space:

$$G_f = \frac{1}{\Omega_0}\int_{\Omega_0} d\Omega_0\, \phi^p \rho_f^n g_f^n \tag{1.6}$$

where g_f^n is the specific Gibbs energy (energy per unit mass) of the interstitial fluid at the pores scale. Using the thermodynamic identity at the pores scale, the specific Gibbs energy may be written in terms of the specific Helmholtz energy ψ_f^n and specific fluid mechanical work w_f^n:

$$g_f^n = \psi_f^n + w_f^n. \tag{1.7}$$

Consecutively, by substitution of (7) in (6) we obtain

$$\begin{aligned} G_f &= \frac{1}{\Omega_0}\int_{\Omega_0} d\Omega_0 \ \left(\phi^p \rho_f^n \psi_f^n + \phi^p \rho_f^n w_f^n\right) \\ &= \Psi_f + \frac{1}{\Omega_0}\int_{\Omega_0} d\Omega_0 \, \phi^p \rho_f^n w_f^n. \end{aligned} \tag{1.8}$$

In addition, the Gibbs energy may be expressed using the thermodynamic identity at the REV scale as follow:

$$G_f = \Psi_f + \phi P_f \tag{1.9}$$

in which ϕP_f stands for the interstitial fluid mechanical work at the REV scale. By identification of equations (8) and (9), we find

$$P_f = \frac{1}{\phi\Omega_0}\int_{\Omega_0} d\Omega_0 \, \phi^p \rho_f^n w_f^n. \tag{1.10}$$

The equation (10) relates the effective pore pressure to the fluid mechanical work at the pore scale. Moreover, (10) ensures that the interstitial fluid mechanical work, expressed in terms of the REV scale variables, equals the actual fluid mechanical work calculated from the nanoscale.

1.4.3 Thermodynamical equilibrium condition

The poromechanical theory distinguishes three sources of dissipation: the skeleton dissipation, the fluid dissipation and the thermal dissipation. The skeleton dissipation Φ_s, is expressed in the lagrangian frame as [5]

$$\Phi_s = \underline{\Sigma} : \frac{d\underline{\Delta}}{dt} - g_f \vec{\nabla}.\vec{M} - S\frac{dT}{dt} - \frac{d\Psi}{dt} \geq 0 \tag{1.11}$$

where $\underline{\Delta}$ is the lagrangian strain tensor, $\vec{M}$ is the lagrangian relative flow vector of fluid mass, T is the temperature, S and Ψ are the global entropy and global Helmholtz free energy of the porous medium {skeleton; interstitial fluid} in the lagrangian frame respectively. This expression of the skeleton dissipation is identical to the one encountered in standard poromechanics. Nevertheless, in the case of the nanoporous continuum, the difference with standard poromechanics lies in the expression of the specific Gibbs energy which involves the effective pore pressure instead of the bulk fluid pressure:

$$g_f = \psi_f + \frac{\phi P_f}{m_f} \tag{1.12}$$

Let us consider now a nanoporous solid immersed in an adiabatic and infinitely rigid container filled with a mass m of fluid. In such conditions, the system {skeleton; interstitial fluid; bulk fluid} is an isolated thermodynamic system. In the limit of reversible transformations, the skeleton dissipation of the open thermodynamic system {skeleton; interstitial fluid} vanishes and we can write

$$\frac{d\Psi}{dt} = \underline{\Sigma} : \frac{d\underline{\Delta}}{dt} - g_f \vec{\nabla}.\vec{M} - S\frac{dT}{dt}. \tag{1.13}$$

The conservation of the interstitial fluid mass is expressed as

$$\frac{dm_f}{dt} + \vec{\nabla}.\vec{M} = 0. \tag{1.14}$$

By identifying the specific Gibbs energy g_f to the chemical potential μ_f of the interstitial fluid, and using (14), we can write the total differential of the Helmholtz free energy of the system {skeleton; interstitial fluid}:

$$d\Psi = \underline{\underline{\Sigma}} : d\underline{\underline{\Delta}} + \mu_f dm_f - SdT. \tag{1.15}$$

The differential of the Helmholtz free energy of the bulk fluid writes as

$$d\Psi_b = -P_b d\phi_b + \mu_b dm_b - S_b dT \tag{1.16}$$

in which ϕ_b is the ratio of the volume occupied by the bulk fluid (*i.e* the volume of the container minus the volume of the porous solid) to the volume of the container. In addition, μ_b, m_b and S_b are the chemical potential, the mass and the entropy of the bulk fluid respectively. The conservation of the total fluid mass $m_t = m_f + m_b$ in the isolated system implies $dm_f = -dm_b$. Therefore, (16) may be rearranged as

$$d\Psi_b = -P_b d\phi_b - \mu_b dm_f - S_b dT. \tag{1.17}$$

The isolated system {skeleton; interstitial fluid; bulk fluid} reaches thermodynamical equilibrium when the global Helmholtz free energy of the system, $\Psi_t = \Psi + \Psi_b$ is minimal. Using relations (15) and (17), we can express the thermodynamical equilibrium condition that must be satisfied by the fluid phase as the equality of the chemical potential of the interstitial fluid and bulk fluid:

$$\mu_f = \mu_b. \tag{1.18}$$

In addition, the chemical potential μ_f of the interstitial fluid at the REV scale, may be obtained by summation of the nanoscale chemical potential μ_f^n over the porous space:

$$\mu_f = \frac{1}{m_f} \int_{\Omega_0} d\Omega_0 \, \phi^p \rho_f^n \mu_f^n. \tag{1.19}$$

The thermodynamical equilibrium condition (18) is then satisfied if $\mu_f^n = \mu_b$. When the system is at equilibrium, the bulk solution is in chemical equilibrium with the interstitial fluid in each pore. Interestingly, the poromechanical model yields the same equilibrium condition as most molecular simulations dealing with pore scale modeling. Indeed, to address the thermodynamical state of fluids at equilibrium, Grand Canonical Monte-Carlo simulation methods assume the equality of the chemical potential throughout the fluid phase [9]. Furthermore, Molecular Dynamics studies on fluid sorption in porous media, which do not impose any *a priori* equilibrium condition, yield results in fair agreement with GCMC methods [21]. As a consequence, the equality of the chemical potentials throughout the fluid phase stands as a consistent thermodynamical equilibrium condition.

1.4.4 Constitutive equation of the effective pore pressure

Accounting for the equation of conservation of the fluid mass (14), a rearranged expression for the skeleton dissipation can be obtained:

$$\Phi_s = \underline{\underline{\Sigma}} : \frac{d\underline{\underline{\Delta}}}{dt} + g_f \frac{dm_f}{dt} - S\frac{dT}{dt} - \frac{d\Psi}{dt} \geq 0. \tag{1.20}$$

We may also write

$$S = S_s + m_f s_f \tag{1.21}$$

$$\Psi = \Psi_s + m_f \psi_f. \tag{1.22}$$

In the limit of reversible transformations (no dissipation), by substituting (12), (21) and (22) in (20), we obtain

$$d\Psi_s = \underline{\Sigma} : d\underline{\Delta} + P_f d\phi - S_s dT. \tag{1.23}$$

This is the general expression of the differential of the Helmholtz free energy of the skeleton.

Now, let ϕ^* be the corrected porosity defined as

$$\phi^* = \frac{1}{\Omega_0} \int_{\Omega_0} d\Omega_0 \, \frac{\rho_f^n}{\rho_b} \phi^p. \tag{1.24}$$

Thus we have $m_f = \rho_b \phi^*$ and by substituting in (12), we obtain a rearranged expression of the thermodynamic identity:

$$g_f = \psi_f + \frac{\phi P_f}{\rho_b \phi^*}. \tag{1.25}$$

By considering the specific Gibbs energy equal to the chemical potential, $g_f = \mu_f$, and if we account for the thermodynamical equilibrium condition (18), then we can re-write the specific Helmholtz free energy of the fluid as follow:

$$\psi_f = \psi_b + \psi_{\text{int}} \tag{1.26}$$

in which ψ_{int} is a specific interaction energy related to the effects of adsorption and molecular packing of fluid molecules in the nanopores, defined as

$$\psi_{\text{int}} = \frac{P_b}{\rho_b} - \frac{P_f}{\rho_b} \left(\frac{\phi}{\phi^*} \right). \tag{1.27}$$

In the same fashion, we can decompose the specific entropy of the interstitial fluid as

$$s_f = s_b + s_{\text{int}} \tag{1.28}$$

in which s_{int} is the interaction entropy due to the effects of adsorption and confinement of fluid molecules in the nanopores. This quantity and the interaction free energy will be discussed further in the last section of this chapter.

In the limit of reversible transformations, by substituting (21), (22), (26), (27) and (28) in (20), we obtain

$$d\Psi_s = \underline{\Sigma} : d\underline{\Delta} - \phi^* dP_b + d(\phi P_f) - (S_s + \rho_b \phi^* s_{\text{int}}) dT \tag{1.29}$$

This is the expression of the Helmholtz free energy of the skeleton in the restricted case of thermodynamical equilibrium of the fluid phase. Upon comparing (29) and (23), we find the constitutive equation of the effective pore pressure and interaction entropy in its incremental form

$$\phi dP_f - \phi^* dP_b - \rho_b \phi^* s_{\text{int}} dT = 0. \tag{1.30}$$

Relation (30) relates the quantities resulting from adsorption and confinement of the fluid molecules, $(P_f \,;\, s_{\text{int}})$, to measurable quantities $(P_b \,;\, T \,;\, \phi \,;\, \phi^*)$. In the limit of isothermal transformations, the incremental constitutive equation reduces to

$$dP_f = \left(\frac{\phi^*}{\phi} \right) dP_b. \tag{1.31}$$

The ratio ϕ^*/ϕ is greater than unity if the mass of interstitial fluid is greater than the mass of bulk fluid occupying the same volume. In other terms, the ratio ϕ^*/ϕ quantifies the degree of confinement of the interstitial fluid. Consecutively, the more the interstitial fluid is confined, the higher the effective pore pressure.

1.4.5 Effect on the volumetric strain

In reversible and isothermal conditions, the differential of the Helmholtz free energy of the nanoporous skeleton is

$$d\Psi_s = \underline{\Sigma} : d\underline{\Delta} + P_f d\phi. \tag{1.32}$$

Classically, in the limit of a reversible response, the constitutive equations read

$$\Sigma_{ij} = \frac{\partial \Psi_s}{\partial \Delta_{ij}} = \left\{(K + b^2 N)\epsilon - bN\phi\right\}\delta_{ij} + 2Ge_{ij} \tag{1.33}$$

$$P_f = \frac{\partial \Psi_s}{\partial \phi} = -bN\epsilon + N\phi \tag{1.34}$$

where $\Delta_{ij} = e_{ij} + (\epsilon/3)\,\delta_{ij}$, K is the apparent modulus of incompressibility, G the shear modulus, b and N the Biot coefficient and modulus respectively.

Consider now that the nanoporous solid is placed in a container filled with a fluid at bulk pressure P_b. As a result, the stress tensor $\underline{\Sigma}$ reduces to the hydrostatic bulk pressure acting on the skeleton:

$$\underline{\Sigma} = -P_b \underline{\mathbb{1}}. \tag{1.35}$$

Moreover, the Biot coefficient is related to the apparent modulus of incompressibility K and to the modulus of the material composing the skeleton matrix K_s:

$$b = 1 - \frac{K}{K_s}. \tag{1.36}$$

From the above relations and from the constitutive equation of the effective pore pressure 31, equations (33) and (34), in their incremental form, yield the volumetric deformation increment, denoted as $d\epsilon$, as a function of the increment of bulk pressure:

$$d\epsilon = \left\{\left(1 - \frac{K}{K_s}\right)\frac{\phi^*}{\phi} - 1\right\}\frac{dP_b}{K}. \tag{1.37}$$

The swelling strain ϵ is obtained by summation of $d\epsilon$ between P_{b0} and P_b:

$$\epsilon - \epsilon_0 = \int_{P_{b0}}^{P_b} \frac{dP_b}{K}\left\{\left(1 - \frac{K}{K_s}\right)\frac{\phi^*}{\phi} - 1\right\} \tag{1.38}$$

1.4.6 Effect on the permeability

In order to arrive at the equivalent of Darcy's Law for nanoporous materials, let us consider the fluid dissipation. In the eulerian frame, it reads [5]

$$\Phi_f^e = \left\{-\vec{\nabla}^e(g_f)_T + (\vec{f} - \vec{\gamma}_f)\right\}.\vec{w} \geq 0 \tag{1.39}$$

where $\vec{\nabla}^e(g_f)_T$ is the eulerian gradient of specific Gibbs energy of the fluid at temperature held constant, $\vec{f}$ and $\vec{\gamma}_f$ are the body force density and fluid acceleration respectively, $\vec{w}$ is the eulerian relative flow vector of fluid mass. Let $\nu = \varphi(\vec{V}_f - \vec{V}_s)$ be the filtration vector in the eulerian frame. The relative flow vector of fluid mass is related to the filtration vector as

$$\vec{w} = \frac{m_f^e}{\varphi}\vec{\nu}. \tag{1.40}$$

By definition, the eulerian fluid mass m_f^e and eulerian porosity φ are related to their lagrangian counterparts as

$$m_f^e d\Omega^e = m_f d\Omega_0 \tag{1.41}$$

$$\varphi d\Omega^e = \phi d\Omega_0. \tag{1.42}$$

Using the above definitions and noting that $m_f = \rho_b \phi^*$, we write the flow vector of mass in terms of the porosity ratio as follows

$$\vec{w} = \rho_b \left(\frac{\phi^*}{\phi} \right) \vec{\nu}. \tag{1.43}$$

In addition, the differential of the specific free energy reads

$$dg_f = \left(\frac{\phi}{\rho_b \phi^*} \right) dP_f - s_f dT. \tag{1.44}$$

By substituting (43) and (44) in (39), we obtain a rearranged expression of the fluid dissipation:

$$\Phi_f^e = \left\{ -\vec{\nabla}^e(P_f) + \rho_b \left(\frac{\phi^*}{\phi} \right) (\vec{f} - \vec{\gamma}_f) \right\} . \vec{\nu}. \tag{1.45}$$

Darcy's law defines a linear relation between the filtration $\vec{\nu}$ and the force that drives the filtration. According to equation (45), Darcy's law reads

$$\vec{\nu} = \kappa \left\{ -\vec{\nabla}^e(P_f) + \rho_b \left(\frac{\phi^*}{\phi} \right) (\vec{f} - \vec{\gamma}_f) \right\} \tag{1.46}$$

where κ is the permeability of the nanoporous material.

Let us consider a bulk pressure gradient driving a flow through a nanoporous membrane, which separates two bulk solutions. In the permanent regime, on each side of the membrane, we assume that the interstitial fluid located at the borders of the nanoporous material is in thermodynamical equilibrium with the neighboring bulk solution. Consecutively, by using equation (30) we relate the bulk pressure differential to the effective pore pressure differential as follows

$$d(P_f)_T = \left(\frac{\phi^*}{\phi} \right) d(P_b)_T \tag{1.47}$$

Substituting 47 in the Darcy law leads to the following expression

$$\vec{\nu} = \kappa_f \left\{ -\vec{\nabla}^e(P_b) + \rho_b (\vec{f} - \vec{\gamma}_f) \right\} \tag{1.48}$$

in which κ_f is the effective permeability of the nanoporous material, defined as

$$\kappa_f = \left(\frac{\phi^*}{\phi} \right) \kappa. \tag{1.49}$$

Therefore, the effective permeability, as it accounts for fluid confinement effects, is greater than the actual permeability κ if the porosity ratio is greater than unity. In other terms, at a given bulk pressure gradient, the more the interstitial fluid is confined, the greater the flux of fluid mass and the greater the effective permeability.

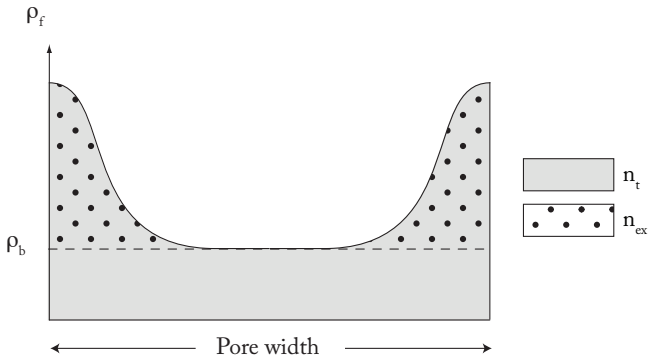

Figure 1.2: Sketch of the fluid density profile in a nanopore. The grey colored area stands for the total number of interstitial fluid n_{t} present in the pore. The dotted area stands for the excess quantity of interstitial fluid which corresponds to the excess number of moles n_{ex} of the Gibbs adsorption isotherm.

1.5 Adsorption induced swelling and permeability change in nanoporous materials

Let us show first how the effective pore pressure, the effective permeability and the swelling strain may be deduced from adsorption measurements. As shown in Figure 2, the Gibbs adsorption isotherm stands as a measurement of the number n_{ex} of adsorbate moles that exceeds the number of fluid molecules at bulk conditions. Let n_{t} be the total number of moles of interstitial fluid (see Figure 2). Then, the ratio of porosities may be expressed as

$$\frac{\phi^*}{\phi} = (1 - n_{\mathrm{ex}}/n_{\mathrm{t}})^{-1} \tag{1.50}$$

so that the effective pore pressure and effective permeability write as

$$P_f - P_{f0} = \int_{P_{b0}}^{P_b} dP_b (1 - n_{\mathrm{ex}}/n_{\mathrm{t}})^{-1} \tag{1.51}$$

$$\kappa_f = (1 - n_{\mathrm{ex}}/n_{\mathrm{t}})^{-1} \kappa \tag{1.52}$$

Equations (51) and (52) show that, at constant bulk pressure, the effective pore pressure and effective permeability increase with the ratio $n_{\mathrm{ex}}/n_{\mathrm{t}}$. In the limit of weak adsorption and weak confinement effects, $n_{\mathrm{t}} \gg n_{\mathrm{ex}}$ as the interstitial fluid is in the same thermodynamical sate as the bulk fluid. In such conditions, equations (51) and (52) indicate that the effective pore pressure and effective permeability equal the bulk fluid pressure and the actual permeability respectively.

Substituting (50) in (38) yields the expression of the volumetric strain as a function of n_{t} and n_{ex}:

$$\epsilon - \epsilon_0 = \int_{P_{b0}}^{P_b} \frac{dP_b}{K} \left\{ \left(1 - \frac{K}{K_s} \right) (1 - n_{\mathrm{ex}}/n_{\mathrm{t}})^{-1} - 1 \right\}. \tag{1.53}$$

Data source	Gas type	m_s (g)	ρ_s $(kg.m^{-3})$	ϕ	K (GPa)	K_s (GPa)
Day et al	CO_2	4.1	1358	0.148	5.64^*	30.1^*
Ottiger et al	CH_4	40.81	1265	0.1379^*	3.0^*	30.1^a
Ottiger et al	CO_2	40.81	1265	0.1194^*	3.0^*	30.1^a

$*$ Adjusted. a Assumed.

Table 1.1: Summary of model parameters for coal swelling

As a result, knowledge of the nanoporous material poroelastic properties K and K_s, and measurement of the sorbed fluid quantities n_{ex} and n_{t} are necessary in order to compute the adsorption induced volumetric strain. Most experimental studies of gas sorption on porous materials focus on the measurement of the Gibbs adsorption isotherm [20]. Experimental adsorption studies do not usually provide the total number of moles of interstitial fluid contained in the porous adsorbent during sorption. The total number of interstitial fluid moles can still be estimated assuming that the porous material undergoes small strains on sorption, which is consistent with most experimental studies found in the literature. Under the approximation of small strains, the porosity of the material can be considered as constant and thus we have

$$\begin{aligned} n_{\text{t}} &\simeq n_{\text{ex}} + \frac{\rho_b V_\phi}{M} \\ n_{\text{t}} &\simeq n_{\text{ex}} + \left(\frac{\phi}{1-\phi}\right)\frac{m_s}{M}\frac{\rho_b}{\rho_s} \end{aligned} \tag{1.54}$$

where V_ϕ is the connected porous volume of the material, M the molar mass of the adsorbed gas, m_s the adsorbent sample mass and ρ_s the density of the material composing the solid matrix of the porous adsorbent. In the following paragraphs, we use relation (54) to compute the total number of interstitial fluid moles from adsorption isotherms data.

Experimental data on the swelling of saturated cement paste are rather scarce in the literature. In order to provide the reader with some validation studies, we are going to focus on carbon dioxyde and methane adsorption in coal. The fluids considered are simple fluids and a typical pore size distribution of coal is not that far from cement paste, with pore sizes in the nanometer range. This setting has the merit of providing a simple configuration on which future models should perform well at least.

1.5.1 Comparison with data from Day and co-workers

[7, 8] performed adsorption experiments and swelling measurements on several Australian bituminous coals. More specifically, they used digital cameras and a pressure cell equipped with sight windows to measure the swelling strain of a Bowen basin coal sample during sorption of carbon dioxide, at $T = 55°C$ and up to $P_b = 15\,\text{MPa}$ [8]. In addition, they performed CO_2 adsorption isotherms measurements on other Bowen basin coal samples at $T = 53°C$ and up to $P_b = 16\,\text{MPa}$ with a gravimetric technique [7]. To compare the theoretical model predictions with the swelling data from [8], we use the adsorption data from [7] corresponding to the Bowen basin coal sample referred to as "Qld 5", whose porosity $\phi = 0.148$ was measured by helium pycnometry. Figure $3(a)$ shows the measured excess adsorption isotherm n_{ex} of CO_2 on the Qld 5 sample as well as the quantity n_{t} deduced from n_{ex} and $\phi = 0.148$ using the relation (54). The volumetric strain is

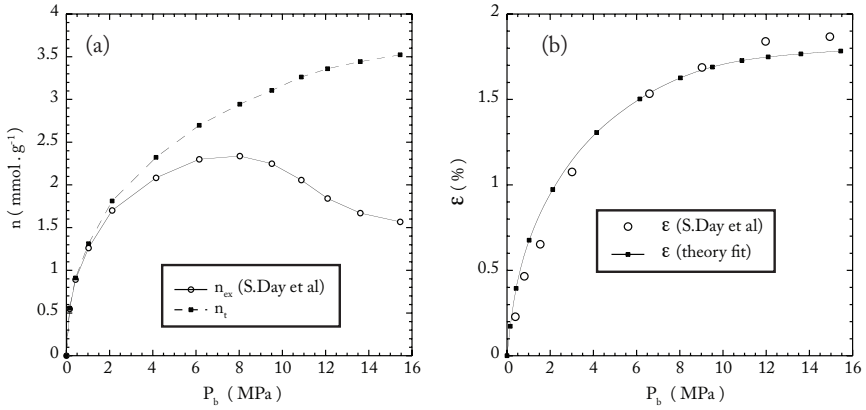

Figure 1.3: (a) Adsorption isotherm of CO_2 on a Bowen basin coal. White circles stand for the excess adsorption isotherm measured by [7]. Black squares stand for the total number of moles of interstitial fluid, computed from n_{ex} data and the value of the coal sample porosity reported in [7]. The lines are guides for the eye. (b) Evolution of the swelling strain with the bulk pressure. White circles stand for the swelling measured by [8]. The black squares represent the fit of the model prediction.The solid line is a guide for the eye.

then computed using equation (38) and fitted to the swelling measurements from [8] with K and K_s as adjustable parameters. Table 1 summarizes the model parameters used in the calculations. Figure 3(b) superposes the experimental data with the fitting curve obtained for $K = 5.64\,\text{GPa}$ and $K_s = 30.1\,\text{GPa}$. For coal, the static Young modulus and Poisson ratio respectively range from 1 GPa to 3 GPa and from 0.25 to 0.45 [25, 10]. Consecutively, the fitted incompressibility modulus of the porous skeleton, $K = 5.64\,\text{GPa}$, falls in the range of the incompressibility modulus of coals. Furthermore, the incompressibility modulus of the solid matrix $K_s = 30.1\,\text{GPa}$ is consistent with the typical value of 35 GPa found in the literature for graphite [12, 4]. In addition, as figure 3(b) demonstrates, the model predicts the evolution of the swelling strain with the bulk pressure in fair agreement with experimental observations.

1.5.2 Comparison with data from Ottiger and co-workers

[17] performed adsorption isotherms measurements of pure CO_2, pure CH_4 and (CO_2, CH_4) mixtures on bituminous coal samples from the Sulcis Province (Italy) at $T = 45°C$ and up to $P_b = 19\,\text{MPa}$, coupling manometric and gravimetric techniques. In addition, they used a pressure cell equipped with sight windows and a digital camera to measure the swelling strain during sorption. In their paper, Ottiger et al. do not report any measurement of the coal samples porosity. As a consequence, we set the solid matrix incompressibility modulus to $K_s = 30.1\,\text{GPa}$, as found in the fitting of the data from S. Day et al, and we fit the model predictions to the swelling data with K and ϕ as adjustable parameters. Figures 4 report the results for pure pure CH_4. The fitted parameters read $K = 3.0\,\text{GPa}$, $\phi = 0.1379$. We observe a good agreement between the theoretical predictions and the experimental data.

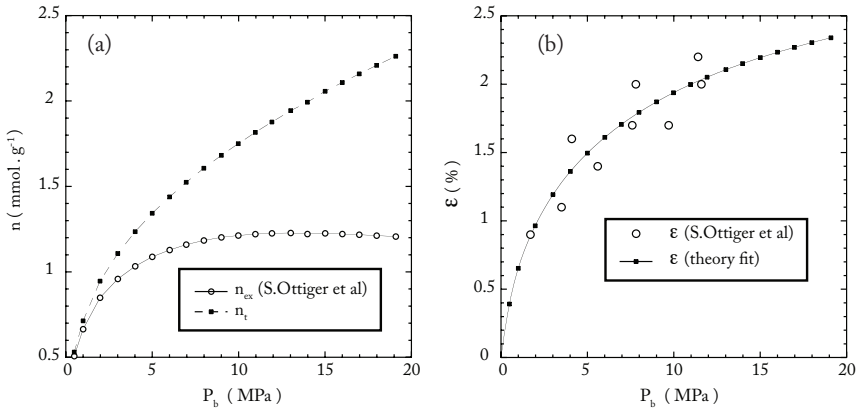

Figure 1.4: (a)Adsorption isotherm of CH_4 on a Sulcis province coal. White circles stand for the excess adsorption isotherm measured by [17]. Black squares stand for the total number of moles of interstitial fluid, computed from the n_{ex} data and the coal sample porosity $\phi = 0.1379$, obtained from the fit of the swelling data. The lines are guides for the eye. (b) Evolution of the swelling strain with the bulk pressure. White circles stand for the swelling measured by [17]. The black squares represent the fit of the model prediction. The solid line is a guide for the eye.

1.5.3 Variation of effective permeability

According to equation (52), the knowledge of the excess number of adsorbed moles n_{ex} and the total number of interstitial fluid moles is necessary to compute the effective permeability. Hence, figure 5 reports the predicted permeability ratio κ_f/κ, calculated from the adsorption data of [7] and [17]. Equation (54) provides an approximation of the total number of interstitial fluid moles. In this figure, we may observe that the effective permeability is always higher than the permeability in the absence of confinement. On the other side, the mass density of the fluid increases with the pressure, which explains why the effective permeability is decreasing with an increase of the bulk pressure.

1.6 Discussion - Interaction energy and entropy

According to equation (26), The specific interaction energy is defined as the difference between the specific Helmholtz energies of the interstitial and bulk fluids when the system reaches equilibrium. If we consider isothermal transformations, equations (27) and (31) show that the sign of the interaction energy is given by the following function F:

$$F(P_b) = f(P_b)P_b - \int_0^{P_b} dP_b f(P_b) \tag{1.55}$$

in which f is the function defined as

$$f(P_b) = \frac{\phi^*}{\phi} = (1 - n_{\text{ex}}/n_{\text{t}})^{-1}. \tag{1.56}$$

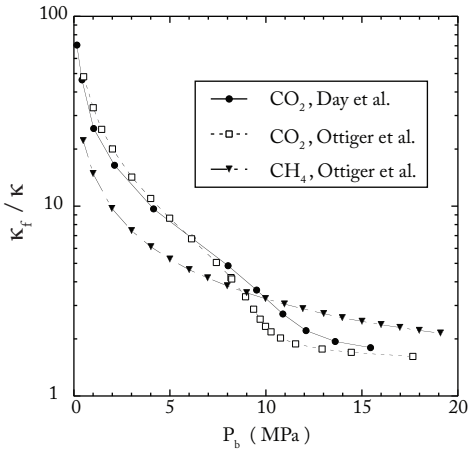

Figure 1.5: Evolution of the permeability ratio κ_f/κ with the bulk pressure in semi-log scale. The permeability ratio is deduced from adsorption data found in the literature: black dots stand for the CO_2 adsorption data from [7]; white squares stand for the CO_2 adsorption data from [17]; black triangles stand for the CH_4 adsorption data from [17]. Lines are guides for the eyes.

The function F is always negative if the function f monotonically decreases with P_b. The derivative of f with respect to P_b reads

$$\frac{df}{dP_b} = (1 - n_{\text{ex}}/n_{\text{t}})^{-2} \frac{d}{dP_b}\left(\frac{n_{\text{ex}}}{n_{\text{t}}}\right). \tag{1.57}$$

Experimental data found in the literature and reported in figures $3(a)$ and $4(a)$ clearly shows that the ratio $n_{\text{ex}}/n_{\text{t}}$ decreases with P_b. Consequently, we deduce from equation (57) that f is a monotonic decreasing function of P_b and thus F is negative. As a result, the interaction energy is negative as well and we find:

$$\psi_f - \psi_b = \psi_{\text{int}} \leq 0. \tag{1.58}$$

Therefore, because of fluid-solid and fluid-fluid interactions in the nanopores, the interstitial fluid cedes free energy to the skeleton under the form of mechanical work, which provokes the swelling phenomenon. When adsorption and confinement effects become negligible, the ratio $n_{\text{ex}}/n_{\text{t}}$ tends to 0 and so does the interaction energy. In such conditions, the interstitial and bulk fluid specific Helmholtz energies are equal.

A simplified poromechanical model which addresses fluid adsorption and molecular packing effects in nanoporous materials has been proposed by Pijaudier-cabot and co-workers [19]. The interaction free energy was introduced directly in the formulation, accounting for the same thermodynamical equilibrium condition and an equivalent form of equation (29) was obtained:

$$d\Psi_s = \underline{\underline{\Sigma}} : d\underline{\underline{\Delta}} + P_b d\phi^* - d\Psi_{\text{int}} \tag{1.59}$$

where Ψ_{int} is the interaction energy, related to the specific interaction energy ψ_{int} as $\Psi_{\text{int}} = m_f \psi_{\text{int}}$. While the approach was quite similar to the present study, the effective pore pressure was not

introduced in this formulation. The interaction energy Ψ_{int} was directly related to the true pore pressure at the pore scale. More specifically, the interaction energy was set as a function of the corrected porosity ϕ^* only, and consecutively an interaction pressure P_{int} was defined as:

$$P_{\text{int}} = \frac{\partial \Psi_{\text{int}}}{\partial \phi^*} \tag{1.60}$$

This interaction pressure plays exactly the same role as the effective pore pressure. A prototype constitutive equation was also postulated:

$$P_{\text{int}} = -k\, n_{\text{ex}} \tag{1.61}$$

where k is a proportionality constant. This empirical constitutive relation was based on the experimental observation of Levine, who pointed out the relation of proportionality between the Gibbs adsorption isotherm and the swelling strain of coal at low bulk pressures [14].

As observed in the comparisons with experimental results, this approximation breaks down at high bulk pressures, as the swelling strain is monotonic whereas the Gibbs adsorption isotherm reaches a maximum and then decreases (see figure 3). Therefore, the knowledge of the adsorbed excess number of moles n_{ex} is not sufficient to accurately predict the pressure inducing the swelling.

Let us now focus on the sign of the interaction entropy s_{int} in the general case of non-isothermal transformations. By rearranging equation (30), we obtain

$$s_{\text{int}} = \frac{1}{\rho_b}\left(\frac{\phi}{\phi^*}\frac{dP_f}{dT} - \frac{dP_b}{dT}\right). \tag{1.62}$$

Several experimental studies point out that the swelling strain, as well as the adsorbed excess number of fluid molecules, decrease upon increasing the temperature [17, 2]. If we consider the paradigm of §0.4.3, these results suggest that the effective pore pressure P_f and the number of bulk fluid moles in the external bulk solution, n_b, respectively decreases and increases with temperature ($dP_f/dT \leq 0$ and $dn_b/dT \geq 0$). Moreover, in the case of small swelling strain, the volume V_b occupied by the external bulk fluid (i.e the volume of the fluid container minus the volume of the porous solid) does not significantly vary upon swelling ($dV_b \simeq 0$). Consecutively, assuming the bulk fluid behaves as an ideal gas, the derivative of the bulk fluid pressure with respect to temperature reads

$$\frac{dP_b}{dT} \simeq \frac{Rn_b}{V_b} + \frac{RT}{V_b}\frac{dn_b}{dT}. \tag{1.63}$$

In such conditions, the bulk fluid pressure increase with temperature ($dP_b/dT \geq 0$). Therefore, considering the above remarks and the expression of the interaction entropy (62), we find:

$$s_{\text{int}} \leq 0. \tag{1.64}$$

By using the definition of the interaction entropy (28), relation (64) leads to

$$s_f \leq s_b. \tag{1.65}$$

This result makes sense as the order in the fluid continuum increases due to the confinement of the fluid molecules in the nanopores, and consecutively, the increase of the fluid density. Thus the interaction entropy quantifies the loss of entropy of the interstitial fluid with respect to the bulk reference state. When adsorption and confinement effects become negligible, as the ratios ϕ/ϕ^* and P_f/P_b asymptotically tends to unity. In these conditions, equation (62) shows that the interaction entropy vanishes.

1.7 Conclusions

We have shown how the poromechanical theory should be refined in the context of saturated isotropic nanoporous solids.

- Because of fluid adsorption and confinement effects in the nanopores, the interstitial fluid pressure is greater than the bulk fluid pressure P_b, which eventually leads to the swelling of the porous solid. We have defined an effective pore pressure P_f in order to account for this effect of adsorption and molecular packing of fluid in small pores.
- When a nanoporous material is immersed in a container filled with a bulk fluid, at thermodynamical equilibrium the interstitial fluid is in chemical equilibrium with the external bulk solution. The chemical potentials throughout the fluid phase are equal.
- In the case of isothermal sorption induced swelling of nanoporous materials, the effective pore pressure P_f has been related to the excess number of adsorbed moles n_{ex}, the total number of moles of interstitial fluid n_{t} and to the bulk pressure P_b.constitutive
- The sorption induced volumetric strain is computed by inserting the effective pressure in the standard poromechanical constitutive equations for the solid phase. A fair agreement between the fit of the theroretical predictions and several sets of experimental data found in the literature is obtained.

Full experimental validation of the model is left for future work, before addressing more complex issues dealing with non satutation of the pores, complex fluids such as water and electrical effects due to the presence of ions in the interstitial solution of cement paste.

1.8 Acknowledgements

The present chapter summarises several results obtained by the authors over the past four years and more extensively described in [16], [13], [19], [23]. It has been partially supported by Total SA under the Tight Gas Project and the European Research Council under Ad-G 27769 Failflow.

Bibliography

[1] D.H. Bangham and N. Fakhroury. The expansion of charcoal accompagnying sorption of gases and vapours. *Nature*, 122:681–682, 1928.

[2] Elisa Battistutta, Patrick van Hemert, Marcin Lutynski, Hans Bruining, and Karl-Heinz Wolf. Swelling and sorption experiments on methane, nitrogen and carbon dioxide on dry Selar Cornish coal. *Int. J. Coal Geol.*, 84(1):39–48, 2010.

[3] F. Beltzung and F. H. Wittmann. Role of disjoining pressure in cement based materials. *Cement and Concrete Research*, 35(12):2364–2370, 2005.

[4] P W Bridgman. The compression of sixty-one solid substances to $25,000\,\mathrm{kg/cm^2}$, determined by a new rapid method. *Proc. Amer. Acad. Arts. Sci.*, 76(1):9–24, 1945.

[5] O. Coussy. *Poromechanics*. John Wiley Pubs, 2004.

[6] O. Coussy. *Mechanics and Physics of Porous Solids*. John Wiley Pubs, 2010.

[7] S Day, G Duffy, R Sakurovs, and S Weir. Effect of coal properties on CO2 sorption capacity under supercritical conditions. *Int. J. Greenh. Gas Con.*, 2(3):342–352, 2008.

[8] S Day, R Fry, and R Sakurovs. Swelling of Australian coals in supercritical CO2. *Int. J. Coal Geol.*, 74(1):41–52, 2008.

[9] Daan Frenkel and Berend Smit. *Understanding molecular simulation*. Academic Press, 2002.

[10] Thomas Gentzis, Nathan Deisman, and R Chalaturnyk. Geomechanical properties and permeability of coals from the foothills and mountain regions of western canada. *Int J. Coal Geol.*, 69(3):153–164, 2007.

[11] Yury Gogotsi, Alexei Nikitin, Haihui Ye, Wei Zhou, John E Fischer, Bo Yi, Henry C Foley, and Michel W Barsoum. Nanoporous carbide-derived carbon with tunable pore size. *Nature mater.*, 2(9):591–4, 2003.

[12] B T Kelly. *Physics of Graphite*. Applied Science Publ., 1981.

[13] A. Knorst-Fouran. *Contribution à l'étude de propriétés interfaciales d'alcanes confinés par simulation moléculaire de type Monte Carlo*. PhD thesis, Université de Pau et des Pays de l'Adour, Septembre 2010.

[14] J. R. Levine. Model study of the influence of matrix shrinkage on absolute permeability of coal bed reservoirs. *Geol. Soc. Spec. Pub.*, 109:197–212, 1996.

[15] F.T. Meehan. The expansion of charcoal on sorption of carbon dioxide. *Proc. R. Soc. A*, 115:199–207, 1927.

[16] B. Mendiboure and C. Miqueu. Evaluation of the pressure tensor of fluids confined into slit micropores. *to be submitted*, 2011.

[17] Stefan Ottiger, Ronny Pini, Giuseppe Storti, and Marco Mazzotti. Competitive adsorption equilibria of co2 and ch4 on a dry coal. *Adsorption*, 14(4-5):539–556, 2008.

[18] V. Pensée, Q.-C. He, and H. Le Quang. Poroelasticity of fluid-infiltrated nanoporous media. *Mater. Sci. Forum*, 614:35–40, 2009.

[19] G. Pijaudier-Cabot, R. Vermorel, C. Miqueu, and B. Mendiboure. Revisiting poromechanics in the context of microporous materials. *C.R. Mecanique, in press*, 2011.

[20] F. Rouquerol, J. Rouquerol, and K. Sing. *Adsorption by powders and porous solids*. Academic Press, 1999.

[21] L Sarkisov and P A Monson. Modeling of adsorption and desorption in pores of simple geometry using molecular dynamics. *Langmuir*, 17(24):7600–7604, 2001.

[22] F. Varnik, J. Baschnagel, and K. Binder. Molecular dynamics results on the pressure tensor of polymer films. *J. Chem. Phys.*, 113(10):4444–4453, 2000.

[23] R. Vermorel and G. Pijaudier-cabot. Poromechanics of saturated isotropic nanoporous materials: a new analytical model for the adsorption induced swelling phenomenon. *Journal of Mech. Phys. Solids, submitted*, 2011.

[24] Kan Yang, Xiancai Lu, Yangzheng Lin, and Alexander V. Neimark. Deformation of Coal Induced by Methane Adsorption at Geological Conditions. *Energ. Fuel.*, 24(11):5955–5964, 2010.

[25] Z Zheng, M Khodaverdian, and J D Mclennan. Static and dynamic testing of coal specimens. In *1991 SCA Conference*, number 9120, 1991.